MARTIN MARIETTA ENERGY SYSTEMS LIBRARIES
3 4456 0364476 9

ORNL-3224
UC-80 – Reactor Technology
TID-4500 (17th ed.)

EFFECTS OF SEISMIC VIBRATIONS ON THE EXPERIMENTAL GAS-COOLED REACTOR

F. J. Witt
D. R. Carver
R. L. Maxwell

CENTRAL RESEARCH LIBRARY
DOCUMENT COLLECTION
LIBRARY LOAN COPY
DO NOT TRANSFER TO ANOTHER PERSON
If you wish someone else to see this document, send in name with document and the library will arrange a loan.

OAK RIDGE NATIONAL LABORATORY
operated by
UNION CARBIDE CORPORATION
for the
U.S. ATOMIC ENERGY COMMISSION

Printed in USA. Price $1.00 Available from the

Office of Technical Services
U. S. Department of Commerce
Washington 25, D. C.

LEGAL NOTICE

This report was prepared as an account of Government sponsored work. Neither the United States, nor the Commission, nor any person acting on behalf of the Commission:

A. Makes any warranty or representation, express or implied, with respect to the accuracy, completeness, or usefulness of the information contained in this report, or that the use of any information, apparatus, method, or process disclosed in this report may not infringe privately owned rights; or

B. Assumes any liabilities with respect to the use of, or for damages resulting from the use of any information, apparatus, method, or process disclosed in this report.

As used in the above, "person acting on behalf of the Commission" includes any employee or contractor of the Commission to the extent that such employee or contractor prepares, handles or distributes, or provides access to, any information pursuant to his employment or contract with the Commission.

ORNL-3224

UC-80 — Reactor Technology
TID-4500 (17th ed.)

Contract No. W-7405-eng-26

Reactor Division

EFFECTS OF SEISMIC VIBRATIONS ON THE EXPERIMENTAL GAS-COOLED REACTOR

F. J. Witt D. R. Carver
R. L. Maxwell

DATE ISSUED

JUN 8 - 1962

OAK RIDGE NATIONAL LABORATORY
Oak Ridge, Tennessee
operated by
UNION CARBIDE CORPORATION
for the
U. S. ATOMIC ENERGY COMMISSION

MARTIN MARIETTA ENERGY SYSTEMS LIBRARIES

3 4456 0364476 9

ABSTRACT

The effects of seismic vibrations on the dynamic behavior of a composite system have been analyzed. The equations of motion were derived and solved with special emphasis on determining the resulting stresses. The method of analysis thus developed was applied to the composite structure consisting of the core, pressure vessel, and supporting skirt of the Experimental Gas-Cooled Reactor (EGCR). A system with three degrees of freedom was considered in order to determine the effects of an earthquake of the maximum intensity expected in the area surrounding Oak Ridge, Tennessee.

The system of equations of motion was solved both numerically and analytically, and the resonant frequencies were determined. The seismic effect was shown to be small when the frequency of the seismic disturbance coincided with a natural frequency of the system. In particular, the shear stresses in the graphite core were shown to be negligible.

CONTENTS

	Page
Nomenclature	vii
1. Introduction	1
2. Equations of Motion Without Damping	2
3. Equations of Motion With Damping	10
4. Solution of the System of Equations	12
5. Seismic Results for the EGCR	18
Appendix A	
Material and Geometrical Constants for the Analysis	27
Verification that Eq. (23) Adequately Approximates Eq. (22)	29
Appendix B	
Analog Solution of the Equations of Motion	30

NOMENCLATURE

A = maximum amplitude of sine wave into which it is assumed graphite columns bend (function of time)

b = vertical distance from lower end of graphite columns to intersection of supporting skirt with reactor vessel

C = bending stiffness of supporting skirt; moment required to give top rim of supporting skirt one radian of angular displacement about any diameter

C_A = damping coefficient for the A degree of freedom

C_θ = damping coefficient for the θ degree of freedom

C_x = damping coefficient for the x degree of freedom

E = modulus of elasticity of graphite

g = acceleration of gravity

G = location of average center of gravity of entire reactor; assumed to be at center of gravity of pressure vessel

h = distance between plane of top rim of support skirt and point G

I = moment of inertia of a cross section of a graphite column with respect to neutral axis of cross section

I_c = mass moment of inertia of core about a horizontal axis through G

I_g = mass moment of inertia of pressure vessel and core about a horizontal axis through G

I_p = mass moment of inertia of pressure vessel about a horizontal axis through G

k_1 = shear stiffness of supporting skirt; force required to displace top rim of supporting skirt a unit distance horizontally with respect to bottom rim

L = length of graphite columns in reactor core

M = total mass of reactor

m_1 = mass of reactor excluding graphite core

m_2 = mass of reactor core

n = number of graphite columns

S = absolute horizontal displacement of earth during an earthquake

x = absolute horizontal displacement of intersection of supporting skirt with reactor vessel; positive to the right; function of time

y = displacement of any point on a graphite column measured perpendicular to a straight line through upper and lower ends of column; positive to the right

z = axis along length of undeflected graphite column measured from lower end of column; positive upward

ρ = mass of reactor core per unit length (m_2/L)

θ = absolute angular rotation of axis of reactor pressure vessel; funtion of time

δ_x = damping factor for the x degree of freedom; i.e., ratio of damping present to critical damping in x coordinate

δ_A = damping factor for the A degree of freedom; i.e., ratio of damping present to critical damping in A coordinate

δ_θ = damping factor for the θ degree of freedom; i.e., ratio of damping present to critical damping in θ coordinate

EFFECTS OF SEISMIC VIBRATIONS ON THE EXPERIMENTAL GAS-COOLED REACTOR

F. J. Witt D. R. Carver*
R. L. Maxwell**

1. Introduction

Seismic disturbances may cause failure or malfunctioning of important components of a nuclear reactor, and, in areas where significant disturbances can be expected to occur, the dynamic behavior of the reactor components must be examined. In particular, the Experimental Gas-Cooled Reactor (EGCR) must be designed to withstand loadings caused by the earthquakes which may occur in the East Tennessee area. The motion of the earth and the accompanying accelerations of the base of a structure during a quake impose both lateral and vertical forces on the supported members. The initiating factor of an earthquake is a sudden shear failure at some dislocation in the earth's crust and subsequent readjustment of the shear stresses from the focal region outward; hence, a disturbance is a response to one or more impulses and is definitely not periodic. In predicting the behavior of a structure under seismic loadings, however, the maximum accelerations for the ground movement and the nature of the response for a body with periodic vibration characteristics to the non-periodic ground motion must be known. Using accelograms from recorded quakes, Biot[1] determined the response of a single-degree-of-freedom ideal oscillator with varying natural periods and found that the maximum acceleration occurred when the period of the oscillator was between 0.1 and 0.5 sec. Particular attention was given to this range of periods in the analysis.

In the absence of adequate data, the U. S. Coast and Geodetic Survey was asked to set a value for the maximum horizontal acceleration to be

---

*Professor, Engineering Mechanics Department, Louisiana State University.

**Professor, Mechanical Engineering Department, University of Tennessee.

[1]M. A. Biot, "Analytical and Experimental Methods in Engineering Seismology," Trans. Am. Soc. Civil Engrs. 108, 365 (1943).

used in designing the EGCR. The value given was 5% of that due to gravity, and the vertical acceleration was taken as one-half this amount. Based on these facts, an analysis was made that considered only horizontal and angular displacements of the composite structure consisting of the core, pressure vessel, and supporting skirt.[2] The nozzles on the pressure vessel and the primary coolant piping were not taken into account, and all the graphite columns were treated as having identical geometries. The graphite columns were assumed to behave under lateral loadings as simply-supported beams, and since graphite is a structurally weak material, special attention was given to the seismic shear stresses in the core. A simple harmonic function was chosen to represent the ground motion.

The equations of motion are derived in Sections 2 and 3, and the exact solution of these equations is obtained for a particular type of disturbance in Sections 4 and 5. Appendix A gives the numerical constants used, and Appendix B presents a comparison of exact and analog computer results. The authors are indebted to B. Y. Cotton who did most of the numerical work associated with this analysis.

2. Equations of Motion Without Damping

The simplified model which includes only the support skirt, pressure vessel, and core of the Experimental Gas-Cooled Reactor is shown in Fig. 1. The reactor building and containment vessel are assumed to follow the motion of the earth, with very little or no buildup of ground acceleration. The pressure vessel is assumed to have horizontal and rotational motion with the top and bottom of the core rigidly fixed to the pressure vessel. As noted above, it is assumed that the graphite columns deflect together as beams simply supported at the ends; hence, it is assumed that they deflect into a sine curve of the form

---

[2] Experimental Gas-Cooled Reactor Preliminary Hazards Summary Report, ORO-196, May 1959. In this report each graphite column was considered to consist of five blocks of equal length fastened together by threaded graphite pins. However, monolithic columns will actually be used, and therefore the analysis described here was made using the monolithic column concept.

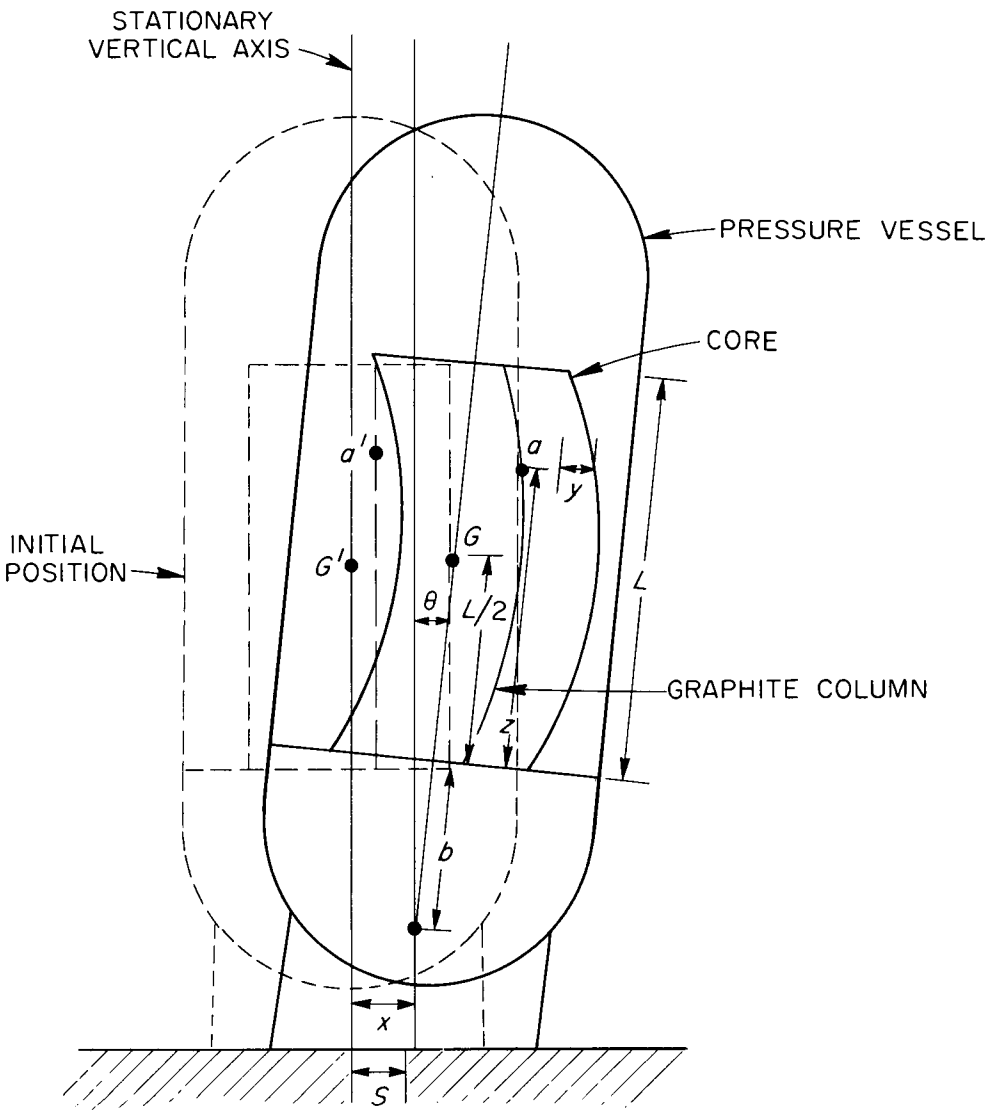

Fig. 1. Model of EGCR Illustrating the Three Degrees of Freedom of Motion.

$$y = A \sin \frac{\pi z}{L} \quad , \tag{1}$$

where A is a function of time. This freedom of movement is illustrated in Fig. 1 by a′, which is the location of a point in the core before a disturbance, and a, which is the instantaneous location of this point after a disturbance. Also G′ and G illustrate the instantaneous displacement

of the center of gravity of the pressure vessel. The absolute horizontal motions for a and G are $x + (b + z)\theta + y$ and $x + [b + (L/2)]\theta$, respectively. A horizontal force-moment diagram for the reactor is shown in Fig. 2, with the external and inertia forces indicated. The deflections are considered to be small. The equations of motion are developed first without considering damping, and the damping effects are then included. Since the seismic restraints are not in actual contact with the pressure vessel, no credit is taken for restraint at their elevations.

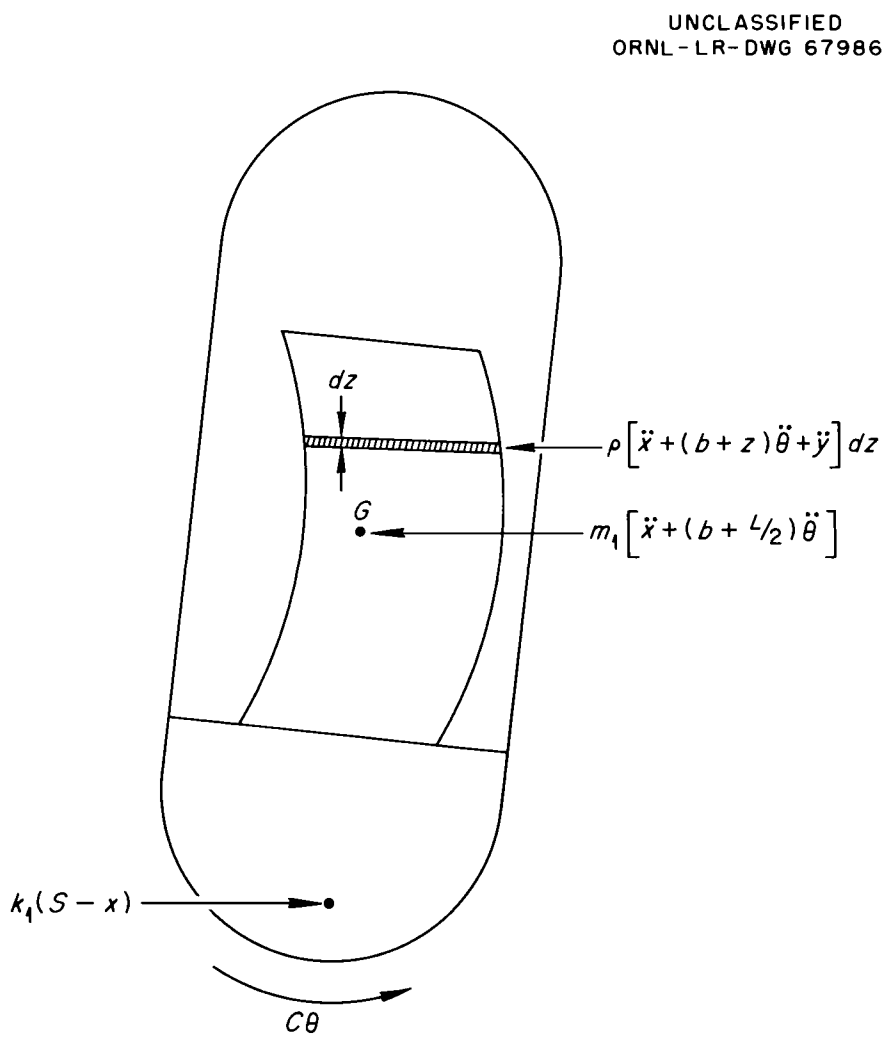

Fig. 2. Horizontal Force-Moment Diagram for the Pressure Vessel and Core.

Summing the horizontal forces in Fig. 2 yields

$$k_1(S - x) = m_1 \left[\ddot{x} + \left(b + \frac{L}{2}\right) \ddot{\theta}\right] + \int_0^L \rho \, [\ddot{x} + (b + z)\ddot{\theta} + \ddot{y}] \, dz \quad , \qquad (2)$$

where the dots denote derivatives with respect to time. Since the deflection is in the form of Eq. (1),

$$\rho \int_0^L [\ddot{x} + (b + z)\ddot{\theta} + \ddot{y}] \, dz = \rho L \left[\ddot{x} + \left(b + \frac{L}{2}\right) \ddot{\theta} + \frac{2}{\pi} \ddot{A}\right] \quad , \qquad (3)$$

and because $\rho L = m_2$, Eq. (2) becomes

$$M\ddot{x} + Mh\ddot{\theta} + \frac{2m_2}{\pi} \ddot{A} + k_1 x = k_1 S \quad , \qquad (4)$$

where $h = b + (L/2)$.

Each graphite column is assumed to be simply supported at the top and bottom, and, in dynamic equilibrium, should satisfy the vibrating beam equation. Thus,

$$EI \frac{\partial^4 y}{\partial z^4} = -\frac{\rho}{n} [\ddot{x} + (b + z)\ddot{\theta} + \ddot{y}] \quad , \qquad (5)$$

where n is the number of graphite columns. When the expression for y is substituted into this equation, it becomes

$$\frac{EI\pi^4}{L^4} A \sin \frac{\pi z}{L} = -\frac{\rho}{n} \left[\ddot{x} + (b + z)\ddot{\theta} + \ddot{A} \sin \frac{\pi z}{L}\right] \quad . \qquad (6)$$

No attempt is made to satisfy the equation at each point z along the axis of the columns. Instead, the total forces along the beams are made to be in equilibrium; that is, both sides of Eq. (6) are integrated with respect to z from 0 to L. The resulting equation is then solved exactly.

Thus[3]

$$2EI \frac{\pi^3}{L^3} A + \frac{m_2}{n} \left[\ddot{x} + \left(b + \frac{L}{2} \right) \ddot{\theta} + \frac{2\ddot{A}}{\pi} \right] = 0 \tag{7}$$

or

$$\frac{m_2}{2n} \ddot{x} + \frac{m_2 h}{2n} \ddot{\theta} + \frac{m_2}{n\pi} \ddot{A} + EI \frac{\pi^3}{L^3} A = 0 \quad . \tag{8}$$

Before deriving the rotation equation, expressions were found for the dynamic shear forces at the top and bottom of the graphite columns. A free-body diagram of the ith column, which is at a distance q_i from the center plane of the pressure vessel, is shown in Fig. 3. The coordinate q_i is considered positive to the right of the center plane. The shearing forces at the top and bottom of the ith column are designated H_{1i} and H_{2i}, respectively. Since the displacements are small, the transverse components of the horizontal forces are considered equal to the forces themselves. Also, the vertical component of displacement of an element of a column is taken to equal $q\theta$ rather than $(q + y)\theta$, since the product $y\theta$ is of second order. In the remaining derivation all nonlinear terms are neglected.

The overturning moment from the shift in the location of the center of gravity of the core is negligible. Also, changes in the moment of inertia of the core from deflection of the core columns are neglected. A summation of the horizontal forces in Fig. 3 yields

$$H_{1i} + H_{2i} = \frac{\rho}{n} \int_0^L [\ddot{x} + (b + z)\ddot{\theta} + \ddot{y}] \, dz \quad . \tag{9}$$

---

[3]The variational procedure with the same assumptions yields a slightly different Eq. (8). The coefficients of the coupling terms, $m_2/2n$ and $m_2h/2n$, are $4m_2/\pi^2 n$ and $4m_2h/\pi^2 n$, respectively, by the variational procedure. Neither equation is exactly correct.

UNCLASSIFIED
ORNL-LR-DWG 67987

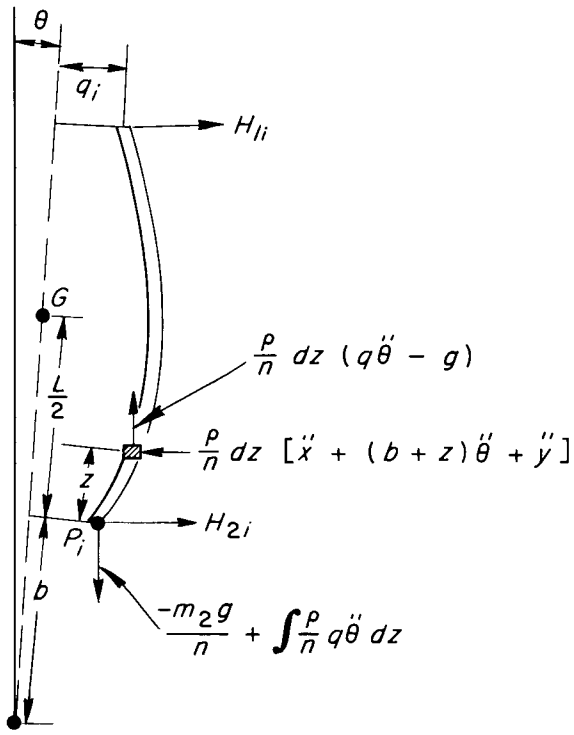

Fig. 3. Free-Body Diagram of a Graphite Column.

As before $\ddot{y} = \ddot{A} \sin(\pi z/L)$ and $\rho L = m_2$, so Eq. (9) becomes

$$H_{1i} + H_{2i} = \frac{m_2}{n}\left[\ddot{x} + \left(b + \frac{L}{2}\right)\ddot{\theta} + \frac{2\ddot{A}}{\pi}\right] . \tag{10}$$

The summation of moments about point P_i, neglecting secondary effects from column bending, yields

$$H_{1i}L = \frac{\rho}{n}\int_0^L [\ddot{x} + (b + z)\ddot{\theta} + \ddot{y}]z\,dz + \frac{\rho}{n}\int_0^L (q_i\ddot{\theta} - g)y\,dz . \tag{11}$$

Hence,

$$H_{1i} = \frac{m_2}{n}\left[\frac{\ddot{x}}{2} + \left(\frac{b}{2} + \frac{L}{3}\right)\ddot{\theta} + \frac{\ddot{A}}{\pi} + \frac{2(q_i\ddot{\theta} - g)A}{\pi L}\right] . \tag{12}$$

Equations (10) and (12) may be combined to give

$$H_{2i} = \frac{m_2}{n}\left[\frac{\ddot{x}}{2} + \left(\frac{b}{2} + \frac{L}{6}\right)\ddot{\theta} + \frac{\ddot{A}}{\pi} - \frac{2(q_i\ddot{\theta} - g)A}{\pi L}\right] \quad . \tag{13}$$

If H_1 and H_2 are the total shear forces at the top and the bottom of the core, respectively, then

$$H_1 = \sum_i H_{1i} \tag{14}$$

and

$$H_2 = \sum_i H_{2i} \quad . \tag{15}$$

Thus, because of symmetry, these shear forces are

$$H_1 = m_2\left[\frac{\ddot{x}}{2} + \left(\frac{b}{2} + \frac{L}{3}\right)\ddot{\theta} + \frac{\ddot{A}}{\pi} - \frac{2gA}{\pi L}\right] \tag{16}$$

and

$$H_2 = m_2\left[\frac{\ddot{x}}{2} + \left(\frac{b}{2} + \frac{L}{6}\right)\ddot{\theta} + \frac{\ddot{A}}{\pi} + \frac{2gA}{\pi L}\right] \quad . \tag{17}$$

These expressions for H_1 and H_2 can now be used to derive the equation of rotational motion. From the free-body diagram shown in Fig. 4, the moments about the center of gravity, G, of the pressure vessel are summed. This gives

$$I_p\ddot{\theta} + C\theta + H_1\frac{L}{2} - H_2\frac{L}{2} - k_1(x - S)\left(b + \frac{L}{2}\right) - Mg\theta\left(b + \frac{L}{2}\right) + \\ + \frac{m_2}{n}\left[\sum_i (q_i\ddot{\theta} - g)q_i\right] = 0 \quad . \tag{18}$$

UNCLASSIFIED
ORNL-LR-DWG 67988

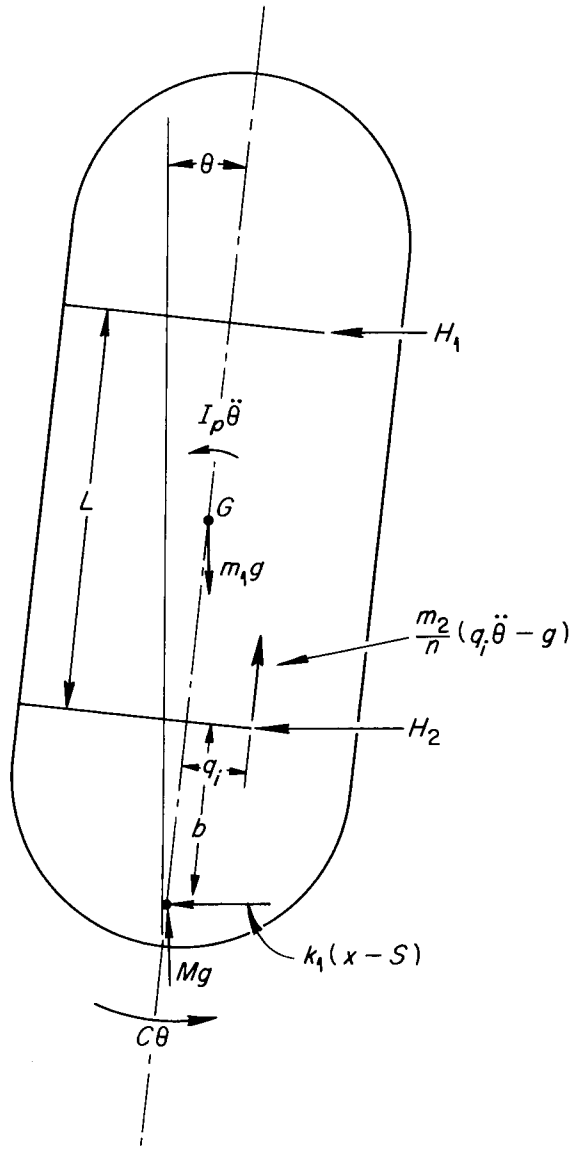

Fig. 4. Free-Body Diagram of the Pressure Vessel.

By substituting for H_1 and H_2, Eq. (18) becomes

$$I_p\ddot{\theta} + m_2\left(\frac{L^2}{12} + \frac{1}{n}\sum_i q_i^2\right)\ddot{\theta} + (C - Mgh)\theta - k_1hx - \frac{2m_2gA}{\pi} = -k_1hS \quad . \qquad (19)$$

In Eq. 19

$$m_2\left(\frac{L^2}{12} + \frac{1}{n}\sum_i q_i^2\right)\ddot{\theta} = \left\{\frac{m_2}{n}\left[\sum_i\left(\frac{L^2}{12} + q_i^2\right)\right]\right\}\ddot{\theta} \quad . \tag{20}$$

Considering the graphite column as a thin rod, $(m_2/n)[(L^2/12) + q_k^2]$ is the moment of inertia of the kth column about the center of gravity of the core. Thus, Eq. (19) becomes

$$(I_p + I_c)\ddot{\theta} + (C - Mgh)\theta - k_1hx - \frac{2m_2gA}{\pi} = -k_1hS \tag{21}$$

or

$$I_G\ddot{\theta} + (C - Mgh)\theta - k_1hx - \frac{2m_2gA}{\pi} = -k_1hS \quad . \tag{22}$$

In Appendix A it is shown that for the case under consideration Mgh and $2m_2gA/\pi$ are small. Thus, Eq. (22) becomes

$$I_G\ddot{\theta} + C\theta - k_1hx = -k_1hS \quad . \tag{23}$$

3. Equations of Motion With Damping

In the previous section an undamped system was considered and the corresponding equations were derived. It will now be assumed that the system is subjected to viscous damping, as indicated in Fig. 5. For each equation of motion the damping coefficient is of the form $2\delta\sqrt{KM}$, where M is the mass of the system described by the equation, K is the spring constant, and δ is the ratio of the actual damping to the critical damping. Thus, in order to include the effects of viscous damping on the equations of motion [Eqs. (4), (8), and (23)], the x coordinate is coupled to the S motion by a retarding force $C_x(\dot{x} - \dot{S})$, the bending

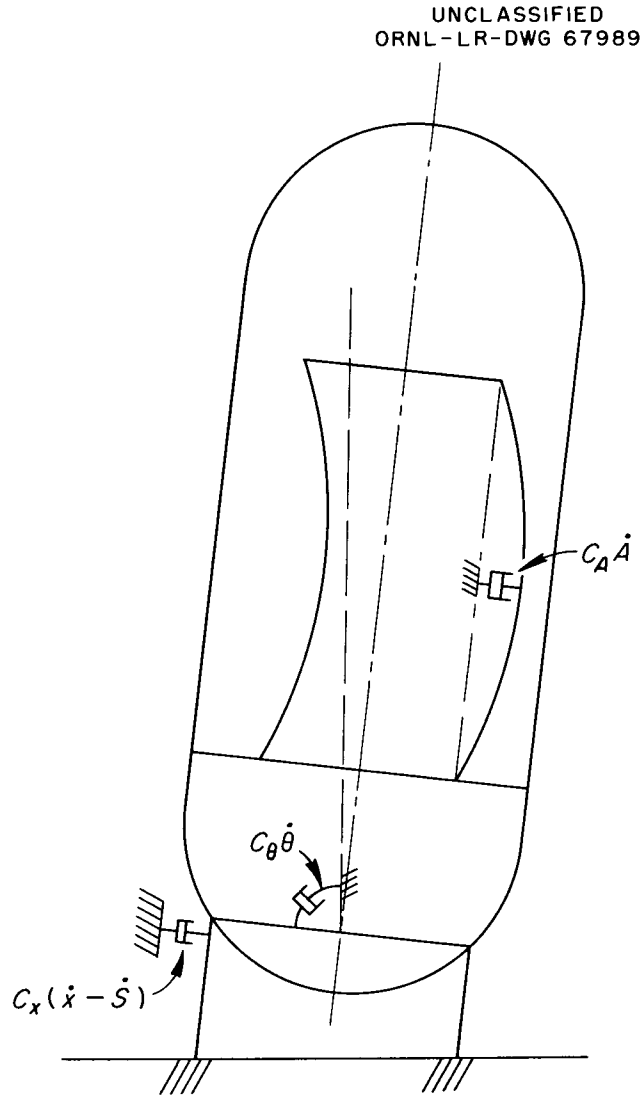

Fig. 5. Damping Diagram for the Pressure Vessel and Core.

vibration is damped by a force $C_A\dot{A}$, and rotation is damped by a force $C_\theta\dot{\theta}$. The coefficients C_x, C_A, and C_θ are given by

$$C_x = 2\delta_x\sqrt{k_1 M} \quad , \tag{24}$$

$$C_A = 2\delta_A\sqrt{\frac{EI\pi^3}{L^3}\,\frac{m_2}{n\pi}} \quad , \tag{25}$$

and

$$C_\theta = 2\delta_\theta \sqrt{CI_G} \quad , \tag{26}$$

where δ_x, δ_A, and δ_θ are the damping factors and are defined as the ratio of the damping present to the critical damping for the x, A, and θ degrees of freedom, respectively.[4] A reasonable range for these damping factors is from 0 to 0.4, and for most structures[4] they are less than 0.2. Since the actual values of these factors are not known, parametric studies were made, as described later.

Thus, the equations of motion become

$$M\ddot{x} + C_x\dot{x} + k_1 x + Mh\ddot{\theta} + \frac{2m_2}{\pi}\ddot{A} = k_1 S + C_x\dot{S} \quad , \tag{27}$$

$$\frac{m_2}{n\pi}\ddot{A} + C_A\dot{A} + \frac{EI\pi^3}{L^3}A + \frac{m_2}{2n}\ddot{x} + \frac{m_2}{2n}h\ddot{\theta} = 0 \quad , \tag{28}$$

and

$$I_G\ddot{\theta} + C_\theta\dot{\theta} + C\theta - k_1 hx = -k_1 hS \quad . \tag{29}$$

4. Solution of the System of Equations

The system of equations was solved using digital computers and the classical method of computation.[5] By this method the natural frequencies are determined, and the transient and steady-state portions of the solution may be separated. The remainder of this section is devoted to a discussion of the solution of the system of equations.

---

[4]F. B. Seely and N. E. Ensign, Analytical Mechanics for Engineers, 4th Edition, John Wiley and Sons, Inc., New York, 1952, pp 368–79.

[5]T. von Karman and M. A. Biot, Mathematical Methods, McGraw-Hill Book Co., Inc., New York, 1940, pp 37–42.

The homogeneous part of the solution is considered first. It is assumed that

$$x_H = D'e^{\alpha t} \quad , \tag{30}$$

$$A_H = F'e^{\alpha t} \quad , \tag{31}$$

and

$$\theta_H = G'e^{\alpha t} \quad , \tag{32}$$

where the subscript H designates the homogeneous portion and D', F', G', and α are constants to be determined. When these expressions are substituted into Eqs. (27), (28), and (29), the following system of linear simultaneous equations in D', F', and G' is obtained.

$$\begin{bmatrix} M\alpha^2 + C_x\alpha + k_1 & \dfrac{2m_2}{\pi}\alpha^2 & Mh\alpha^2 \\ \dfrac{m_2}{2n}\alpha^2 & \dfrac{m_2}{n\pi}\alpha^2 + C_A\alpha + \dfrac{EI\pi^3}{L^3} & \dfrac{m_2 h\alpha^2}{2n} \\ -k_1 h & 0 & I_G\alpha^2 + C_\theta\alpha + C \end{bmatrix} \begin{bmatrix} D' \\ F' \\ G' \end{bmatrix} = \begin{bmatrix} 0 \\ 0 \\ 0 \end{bmatrix} \tag{33}$$

For a nontrivial solution to exist, the determinant of the matrix must be zero. This yields a sixth-degree polynomial in α and is called the characteristic equation. Thus

$$P_1\alpha^6 + P_2\alpha^5 + P_3\alpha^4 + P_4\alpha^3 + P_5\alpha^2 + P_6\alpha + P_7 = 0 \quad , \tag{34}$$

where

$$P_1 = \left(\frac{Mm_2}{n\pi} - \frac{m_2^2}{n\pi}\right) I_G \quad , \tag{35}$$

$$P_2 = \frac{m_2 I_G}{n\pi} C_x + MI_G C_A + \left(\frac{Mm_2}{n\pi} - \frac{m_2^2}{n\pi}\right) C_\theta \quad , \tag{36}$$

$$P_3 = \left(\frac{MEI\pi^3}{L^3} + \frac{k_1 m_2}{n\pi}\right) I_G + \left(\frac{Mm_2}{n\pi} - \frac{m_2^2}{n\pi}\right) C +$$

$$+ (Mm_2 - m_2^2) \frac{k_1 h^2}{n\pi} + I_G C_x C_A + MC_A C_\theta + \frac{m_2}{n\pi} C_x C_\theta \quad , \tag{37}$$

$$P_4 = \left(\frac{EI\pi^3 I_G}{L^3} + \frac{m_2}{n\pi} C\right) C_x + (k_1 I_G + MC + k_1 Mh^2) C_A +$$

$$+ \left(\frac{MEI\pi^3}{L^3} + k_1 \frac{m_2}{n\pi}\right) C_\theta + C_x C_A C_\theta \quad , \tag{38}$$

$$P_5 = \left(k_1 \frac{EI\pi^3}{L^3} + \frac{MEI\pi^3}{L^3} C\right) I_G + k_1 \frac{m_2}{n\pi} C + k_1 \frac{Mh^2 EI\pi^3}{L^3} +$$

$$+ \frac{EI\pi^3}{L^3} C_x C_\theta + k_1 C_A C_\theta + CC_x C_A \quad , \tag{39}$$

$$P_6 = \frac{EI\pi^3}{L^3} CC_x + k_1 CC_A + k_1 \frac{EI\pi^3}{L^3} C_\theta \quad , \tag{40}$$

$$P_7 = k_1 \frac{EI\pi^3}{L^3} C \quad . \tag{41}$$

Each root of the polynomial guarantees the existence of a solution. Hence, the complete homogeneous solution becomes

$$x_H = \sum_{j=1}^{6} D_j e^{\alpha_j t} \quad , \tag{42}$$

$$A_H = \sum_{j=1}^{6} F_j e^{\alpha_j t} \quad , \tag{43}$$

$$\theta_H = \sum_{j=1}^{6} G_j e^{\alpha_j t} \quad . \tag{44}$$

The 18 constants of integration are reduced to six by solving two of the equations in the system for two of the unknowns, D_j and F_j, for example, in terms of the third, G_j. This gives

$$D_j = \frac{I_G \alpha_j^2 + C_\theta \alpha_j + C}{k_1 h} G_j \tag{45}$$

$$F_j = -\frac{\pi}{2m_2}\left[Mh + \frac{1}{k_1 h}\left(MI_G\alpha_j^2 + MC_\theta\alpha_j + MC + I_G C_x \alpha_j + \right.\right.$$
$$\left.\left. + C_x C_\theta + \frac{C_x C}{\alpha_j} + k_1 I_G + \frac{k_1 C_\theta}{\alpha_j} + \frac{k_1 C}{\alpha_j^2}\right)\right] G_j \quad . \tag{46}$$

The roots of Eq. (34) occur in complex conjugate pairs of the form

$$\alpha_j = \tau_j \pm i\sigma_j \quad . \tag{47}$$

When the expressions given in Eqs. (45), (46), and (47) are used in Eqs. (42), (43), and (44), the following set of equations is obtained:

$$x_H = \sum_{j=1}^{3} e^{\tau_j t} (H_j \cos \sigma_j t - I_j \sin \sigma_j t) \quad , \tag{48}$$

$$A_H = \sum_{j=1}^{3} e^{\tau_j t} (J_j \cos \sigma_j t - K_j \sin \sigma_j t) \quad , \tag{49}$$

$$\theta_H = \sum_{j=1}^{3} e^{\tau_j t} (L_j \cos \sigma_j t - M_j \sin \sigma_j t) \quad , \tag{50}$$

where

$$H_j = (2D_j)_R \quad , \tag{51}$$

$$I_j = (2D_j)_I \quad , \tag{52}$$

$$J_j = (2F_j)_R \quad , \tag{53}$$

$$K_j = (2F_j)_I \quad , \tag{54}$$

$$L_j = (2G_j)_R \quad , \tag{55}$$

$$M_j = (2G_j)_I \quad . \tag{56}$$

The subscripts R and I signify the real and imaginary parts, respectively, which are obtained[6] by using the plus sign in Eq. (47). It should be noted that the real parts of the roots of the characteristic equation are the damping exponents and the imaginary parts are the resonant frequencies.

The forcing function, S, is assumed to be of the form

$$S = \sum_k S_k \cos (w_k t + \phi_k) \quad . \tag{57}$$

Since the system of equations is linear, particular solutions are additive. Thus, only one term of Eq. (57) needs to be considered. Subscripts p will denote particular solutions. If

---

[6]A real forcing function will be used; hence, the solutions are real and the results given here follow.

$$S = S_0 \cos (w_0 t + \phi_0) = (S_0 \cos \phi_0) \cos w_0 t - $$
$$- (S_0 \sin \phi_0) \sin w_0 t \quad , \tag{58}$$

then the particular solutions are of the form

$$x_p = N_0 \cos w_0 t + O_0 \sin w_0 t \tag{59}$$

$$A_p = P_0 \cos w_0 t + Q_0 \sin w_0 t \tag{60}$$

$$\theta_p = R_0 \cos w_0 t + T_0 \sin w_0 t \quad . \tag{61}$$

By substituting Eqs. (59), (60), and (61) into the system of equations, a linear simultaneous system results that is given here in matrix form.

$$\begin{bmatrix} -Mw_0^2 + k_1 & C_x w_0 & -\frac{2m_2}{\pi} w_0^2 & 0 & -Mhw_0^2 & 0 \\ C_x w_0 & Mw_0^2 - k_1 & 0 & \frac{2m_2}{\pi} w_0^2 & 0 & Mhw_0^2 \\ -\frac{m_2 w_0^2}{2n} & 0 & -\frac{m_2 w_0^2}{n\pi} + \frac{EI\pi^3}{L^3} & C_A w_0 & -\frac{m_2}{2n} hw_0^2 & 0 \\ 0 & -\frac{m_2}{2n} w_0 & -C_A w_0 & -\frac{m_2}{n\pi} w_0^2 + \frac{EI\pi^3}{L^3} & 0 & -\frac{m_2 hw_0^2}{2n} \\ -k_1 h & 0 & 0 & 0 & -I_G w_0^2 + C & C_\theta w_0 \\ 0 & -k_1 h & 0 & 0 & -C_\theta w_0 & -I_G w_0^2 + C \end{bmatrix} \begin{bmatrix} N_0 \\ O_0 \\ P_0 \\ Q_0 \\ R_0 \\ T_0 \end{bmatrix} = \begin{bmatrix} S_0(k_1 \cos \phi - \\ \quad - C_x w_0 \sin \phi) \\ S_0(k_1 \sin \phi + \\ \quad + C_x w_0 \cos \phi) \\ 0 \\ 0 \\ -k_1 h S_0 \cos \phi \\ k_1 h S_0 \sin \phi \end{bmatrix} \tag{62}$$

The solution of this system yields the particular solution. Thus, particular solutions are of the form

$$x_p = \sum_k (N_k \cos w_k t + O_k \sin w_k t) \tag{63}$$

$$A_p = \sum_k (P_k \cos w_k t + Q_k \sin w_k t) \tag{64}$$

$$\theta_p = \sum_k (R_k \cos w_k t + T_k \sin w_k t) \quad . \tag{65}$$

The complete general solution is then

$$x = \sum_{j=1}^{3} e^{\tau_j t} (H_j \cos \sigma_j t - I_j \sin \sigma_j t) +$$

$$+ \sum_k (N_k \cos w_k t + O_k \sin w_k t) \tag{66}$$

$$A = \sum_{j=1}^{3} e^{\tau_j t} (J_j \cos \sigma_j t - K_j \sin \sigma_j t) +$$

$$+ \sum_k (P_k \cos w_k t + Q_k \sin w_k t) \tag{67}$$

$$\theta = \sum_{j=1}^{3} e^{\tau_j t} (L_j \cos \sigma_j t - M_j \sin \sigma_j t) +$$

$$+ \sum_k (R_k \cos w_k t + T_k \sin w_k t) \quad . \tag{68}$$

For the problem under study, the initial conditions on the general solution are

$$x = A = \theta = \dot{x} = \dot{A} = \dot{\theta} = 0 \quad . \tag{69}$$

5. Seismic Results for the EGCR

A listing of the constants which apply to this analysis and an explanation of how some of these constants were derived is given in Appendix A. Substituting the constants into Eqs. (27), (28), and (29) yields

$$\ddot{x} = 19.083\ddot{\theta} + 0.1946\ddot{A} + 410.82\delta_x\dot{x} + $$
$$+ 42193x = 410.82\delta_x\dot{S} + 42193S \qquad (70)$$

$$\ddot{x} + 19.083\ddot{\theta} + 0.6366\ddot{A} + 86.321\delta_A\dot{A} + 3043A = 0 \qquad (71)$$

$$\ddot{\theta} + 323.32\delta_\theta\dot{\theta} + 26134\theta - 6546x = -6546S \quad . \qquad (72)$$

As previously noted, the damping factors must be considered as parameters. Various combinations of these factors were taken and corresponding damping exponents and damped natural frequencies were found. The results of this procedure are shown in Table 1. Theoretical analyses have shown that considerable damping is required to alter noticeably the natural frequencies of structures of this type. This is borne out in Table 1.

While Eq. (57), considered as a Fourier series, could be made to describe <u>any</u> random motion, such a consideration may not be necessary. Should the impressed frequency coincide with a natural frequency,

Table 1. Natural Frequencies and Damping Exponents for Certain Damping Factors

Damping Factors			Real and Imaginary Parts of Characteristic Equation (Damping Exponents and Natural Frequencies)		
δ_x	δ_A	δ_θ			
0	0	0	(0, 58.53)[a]	(0, 102.1)	(0, 452.3)
0.03	0.03	0.03	(−1.318, 58.52)	(−3.45, 101.98)	(−11.89), 452.2)
0.05	0.05	0.05	(−2.196, 58.49)	(−5.749, 101.8)	(−19.81, 452.1)
0.1	0.1	0.1	(−4.388, 58.38)	(−11.49, 101.22)	(−39.64, 451.3)
0.4	0.4	0.4	(−16.72, 59.88)	(−45.91, 81.37)	(−159.4, 437.0)
0.01	0.15	0.01	(−4.896, 58.98)	(−9.172, 100.5)	(−5.155, 452.2)
0.05	0.1	0.05	(−3.772, 58.54)	(−8.631, 101.4)	(−20.24, 451.99)
0.05	0.15	0.05	(−5.367, 58.71)	(−11.50, 100.7)	(−20.66, 451.9)
0.1	0.2	0.1	(−7.567, 58.60)	(−17.24, 99.52)	(−40.47, 450.9)
0.15	0.2	0.1	(−7.828, 58.44)	(−18.27, 99.54)	(−53.98, 449.6)

[a]The first number of each pair is the damping exponent and the second number is the natural frequency in radians per second.

amplitudes of the forced vibration should approach maximum values. The ground accelerations associated with an earthquake may be larger than those predicted by the U. S. Coast and Geodetic Survey, and the most important feature of the structure is that there must not be large magnifications of the displacement amplitudes when resonances occur. Hence, a forcing function with a frequency near that of the natural frequency for the structure was used in this investigation.

In the solution that follows the damping factors were 5, 15, and 5% of critical for the x, A, and θ coordinates, respectively.[7] For this case the natural frequencies are 9.3, 16.0, and 71.9 cycles per second (58.71, 100.7, and 451.9 radians per second). For the forcing function, Eq. (57), S_k, w_k, and ϕ were chosen so that resonance existed at the lowest natural frequency, and the maximum acceleration was 0.05 g, that is,

$$S = -4.670 \times 10^{-4} \cos 58.71\ t \quad . \tag{73}$$

The displacement as a function of time is plotted for each of the coordinates in Figs. 6, 7, and 8. Figures 9, 10, and 11 are similar plots for the accelerations. Since A is the maximum displacement at the midplane of a graphite column, it is proportional to the maximum bending stress, as indicated by the ordinate on the right in Fig. 7. It is particularly interesting to note in this graph that the curve builds up to the steady state; this suggests that 9.3 cps is the fundamental frequency associated with the motion of the graphite columns in the system as a whole. Figures 12 and 13 show the total shear forces at the top and bottom of the core, as given by Eqs. (16) and (17). The ordinate on the right indicates the resulting shear stress. In each of the graphs the transient and steady-state solutions were found separately and then added to give the general solution, as indicated. Only a short time interval

[7]These values seemed reasonable after considering Edward Y. W. Tsui, "Aseismic Design of Structures by Rigidity Criterion," Journal of the Structural Division, Proceedings of the ASCE, February 1960, pp 81–106.

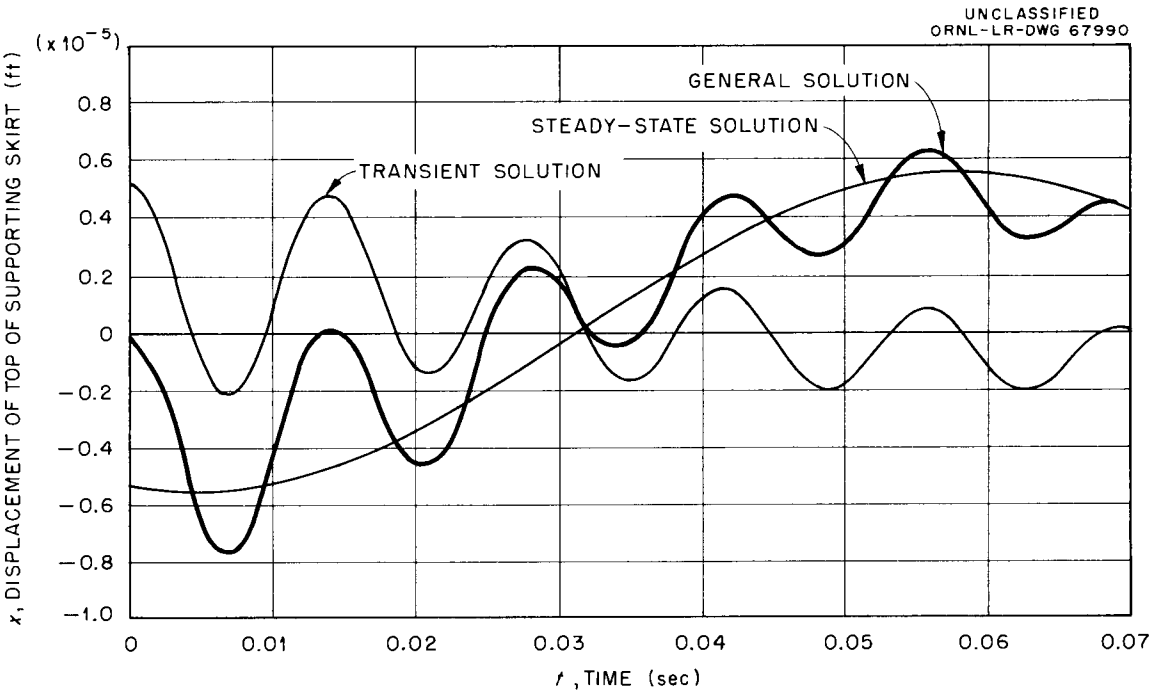

Fig. 6. Time-Dependent Displacement of the Top of the Supporting Skirt.

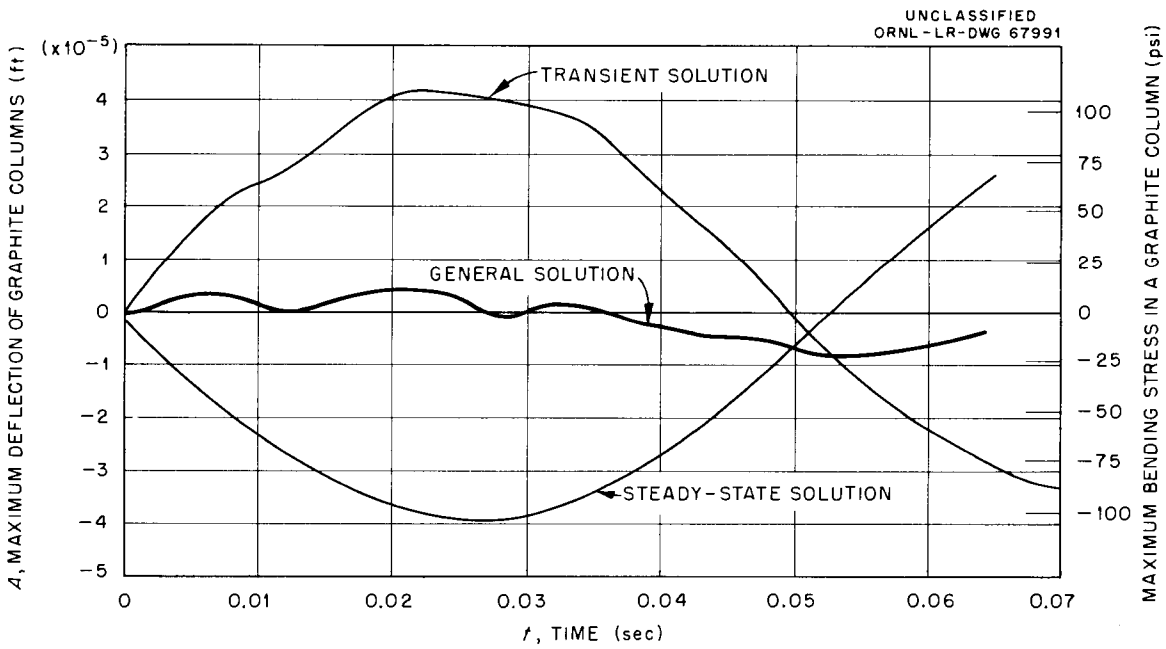

Fig. 7. Time-Dependent Maximum Deflection and Bending Stress in Graphite Columns.

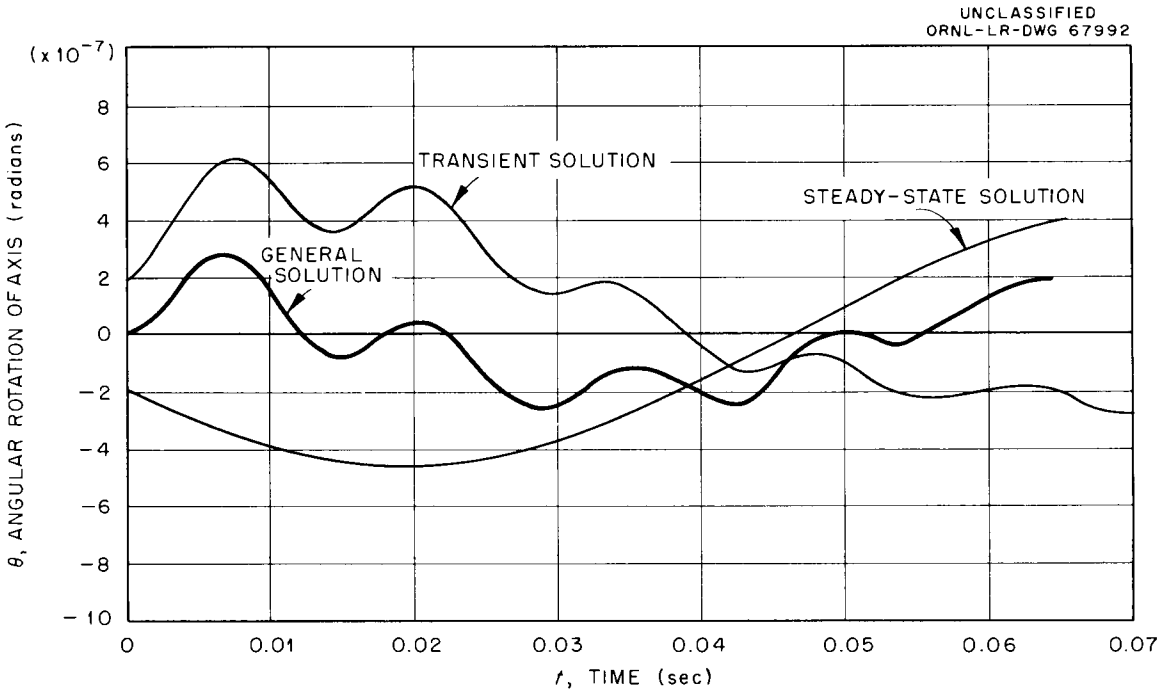

Fig. 8. Time-Dependent Angular Rotation of the Axis of the Pressure Vessel.

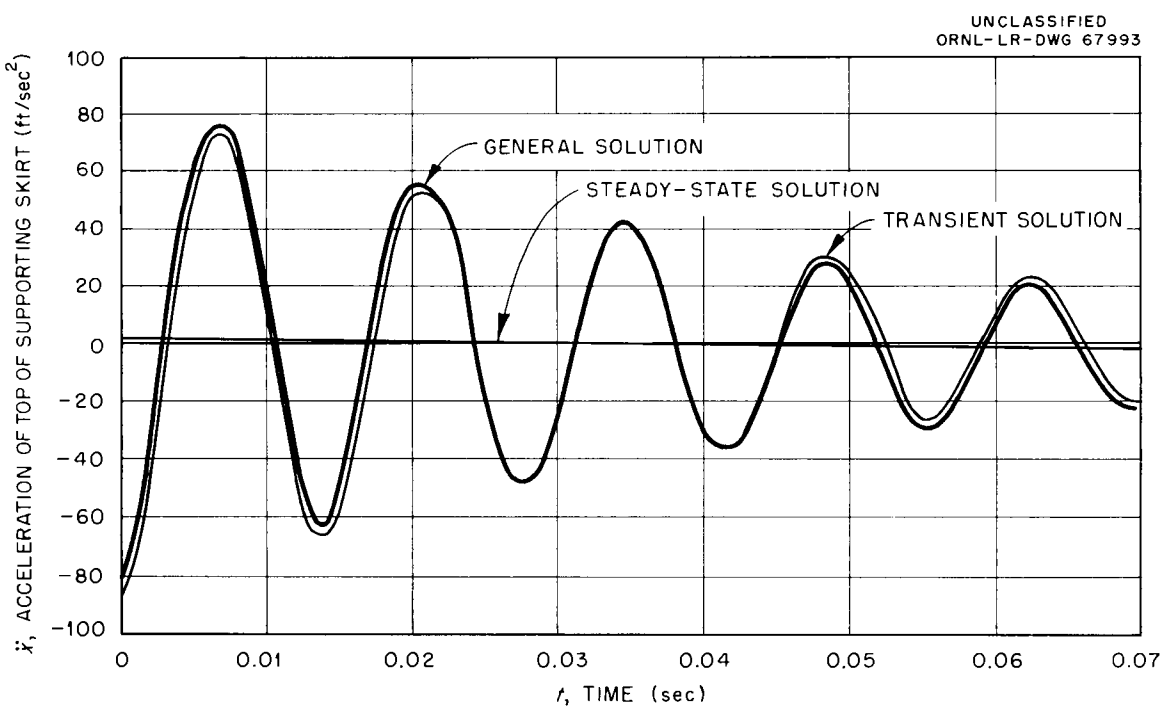

Fig. 9. Time-Dependent Acceleration of the Top of the Supporting Skirt.

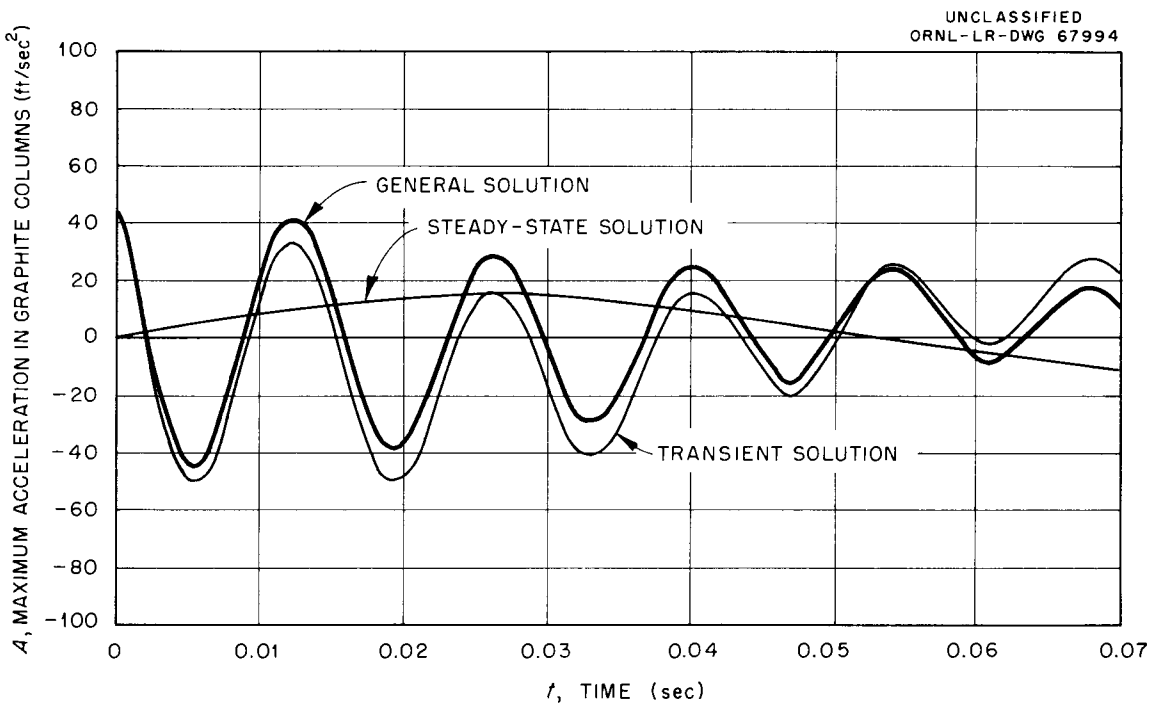

Fig. 10. Time-Dependent Maximum Acceleration in Graphite Columns.

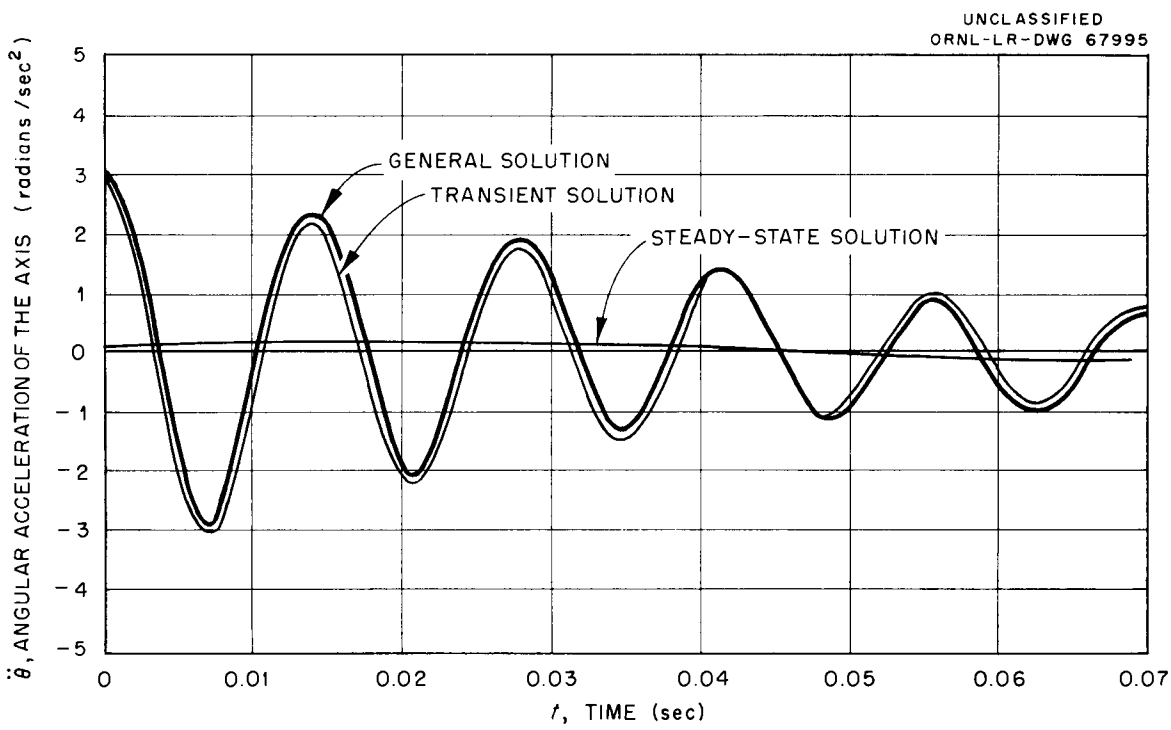

Fig. 11. Time-Dependent Angular Acceleration of the Axis of the Pressure Vessel.

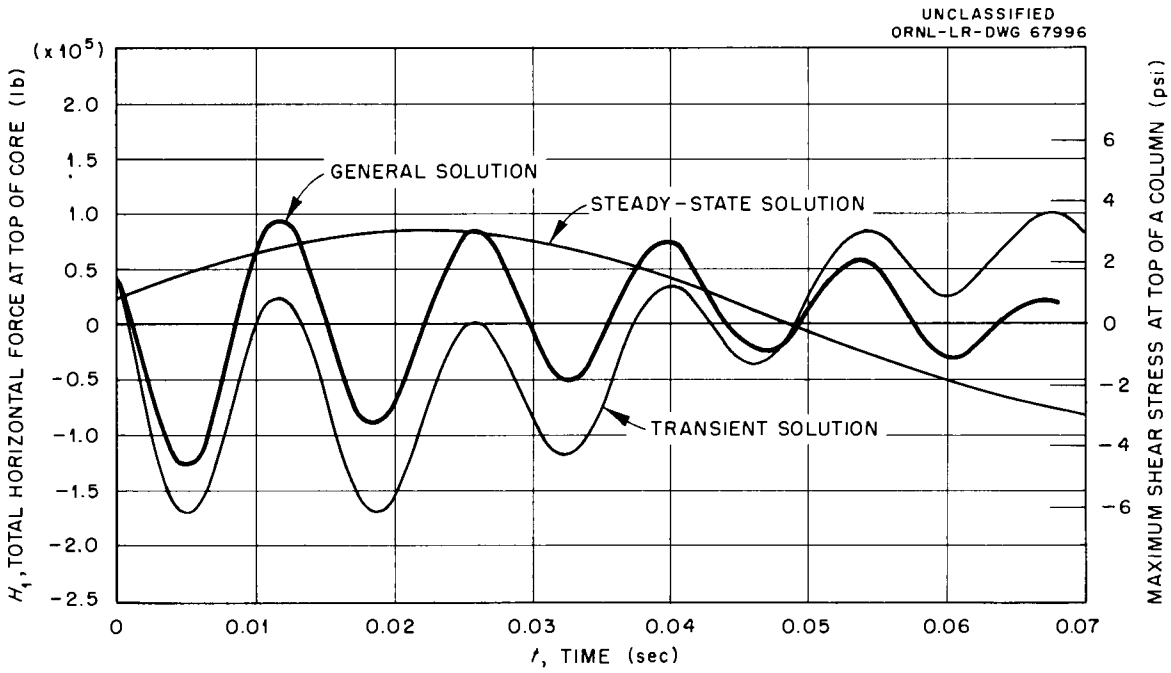

Fig. 12. Time-Dependent Total Horizontal Force at Top of Core and Maximum Shear Stress at Top of a Column.

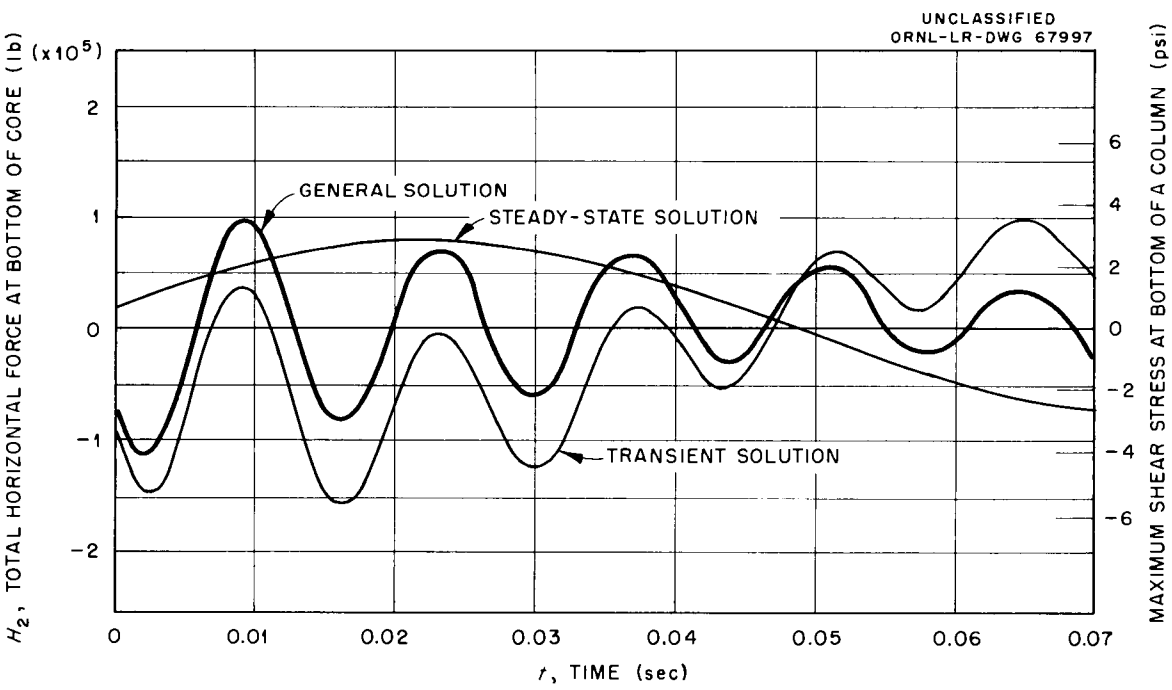

Fig. 13. Time-Dependent Total Horizontal Force at Bottom of Core and Maximum Shear Stress at Bottom of a Column.

is plotted because the transient solution has its maximum effect very early and then dries out.

A summary of the results produced by the forcing function of Eq. (73) is presented below:

max $x = 7.7 \times 10^{-4}$ ft max $\ddot{x} = 88$ ft/sec^2

max $A = 40 \times 10^{-4}$ ft max $\ddot{A} = 46$ ft/sec^2

max $\theta = 46 \times 10^{-6}$ rad max $\ddot{\theta} = 3$ rad/sec^2

max $H_1 = 130\ 000$ lb max $H_2 = 115\ 000$ lb

max shear stress = 5 psi max bending stress = 105 psi

max displacement of the top of the support skirt with respect to the ground = 4.6703×10^{-4} ft

max displacement of the top of the pressure vessel with respect to the ground = 4.6703×10^{-4} ft

Steady-state solutions were found for several frequencies, and representative values are presented in Table 2 as comparisons of the ratios of the steady-state displacements and accelerations to the ground displacement and acceleration for frequencies of 1.3, 58.71, and 100.7 radians/sec. A similar table resulting from an analysis on an analog computer is given in Appendix B. It may be seen from Table 2 that there is no serious magnification of amplitudes when resonance occurs between the ground and structure motions.

The forcing function used does not represent the disturbances caused by recorded quakes. However, the magnitudes of the stresses and displacements corresponding to the forcing function used were very small

Table 2. Comparison of the Ratios of the Maximum Steady-State Displacements and Accelerations to the Maximum Ground Displacement and Acceleration for Three Frequencies

Frequency (radians/sec)	$\frac{\max x}{\max S}$ or $\frac{\max \ddot{x}}{\max \ddot{S}}$	$\frac{\max A}{\max S}$ or $\frac{\max \ddot{A}}{\max \ddot{S}}$	$\frac{\max \theta(\text{radians})}{\max S}$ or $\frac{\max \ddot{\theta}(\text{radians})}{\max S}$
1.3	1.00004	0.00056	0.00001
58.71	1.19	8.4	0.097
100.7	0.93	5.05	0.095

despite the selection of a frequency very near the natural frequency of the system. In view of this, a more accurate representation of a true earthquake disturbance was not warranted.

On the basis of the low stresses (summarized above) found in this study, it is concluded that, under the assumptions made, the stresses induced by predicted seismic disturbances alone present no hazard to the EGCR. It is interesting to note that for the forcing function with a frequency of 58.71 radians/sec a ground acceleration of about 0.5 g (based on the measured flexure strength of approximately 1000 psi) would be necessary to fracture the graphite columns.

APPENDIX A

Material and Geometrical Constants for the Analysis

Listed below are the constants for the EGCR that were used to solve Eqs. (27), (28), and (29):

$$M = 1.4065 \times 10^6 \text{ lb} = 4.368 \times 10^4 \text{ slugs}$$
$$m_2 = 0.43 \times 10^6 \text{ lb} = 1.3354 \times 10^4 \text{ slugs}$$
$$\frac{m_2}{n} = 119.925 \text{ slugs}$$
$$L = 19 \text{ ft } 4 \text{ in.}$$
$$h = 19 \text{ ft } 1 \text{ in.}$$
$$I_G = 5.373 \times 10^6 \text{ slug}\cdot\text{ft}^2$$
$$I = 3927 \text{ in.}^4$$
$$C = 14.042 \times 10^{10} \text{ ft}\cdot\text{lb/radian}$$
$$k_1 = 1843 \times 10^6 \text{ lb/ft}$$
$$E = 1.5 \times 10^6 \text{ psi}$$
$$C_x = 17.9446 \times 10^6 \ \delta_x$$
$$C_A = 51.7604 \times 10^4 \ \delta_A$$
$$C_\theta = 17.372 \times 10^8 \ \delta_\theta$$

Most of these values are known explicitly;[1] the remaining are discussed below.

The graphite columns for the EGCR are monolithic structures with 16-in. × 16-in. quasi-square cross sections. They are 232 in. long with a weight per unit length of 10.09 lb. The eight dummy fuel assemblies in the ends of the fuel channels were assumed to weigh 50 lb each. The 24 fuel elements, each weighing 47.6 lb, were assumed to be distributed over the rest of the length of the channel.

The moment of inertia, I_G, of the pressure vessel and core about the center of gravity of the pressure vessel was found by summing the moments of inertia about the point for the following components: the core, the

[1]Experimental Gas-Cooled Reactor Preliminary Hazards Summary Report, ORO-196 (May 1959).

lower grid and grid plate, the upper grid and grid plate, the cylindrical shell of the pressure vessel, and the upper and lower hemispheres of the pressure vessel.

The support skirt constants, C and k_1, were calculated from Fig. A.1. The skirt was assumed to be at a temperature of 500°F and to have a modulus of elasticity of 28×10^6 psi. Poisson's ratio, μ, was taken as 0.3. The shear strain, γ, is given by

$$\gamma = \frac{F}{AG} ,$$

where A is the cross-sectional area of the skirt, F is the horizontal force, and

$$G = \frac{E}{2(1 + \mu)} .$$

UNCLASSIFIED
ORNL-LR-DWG 67998

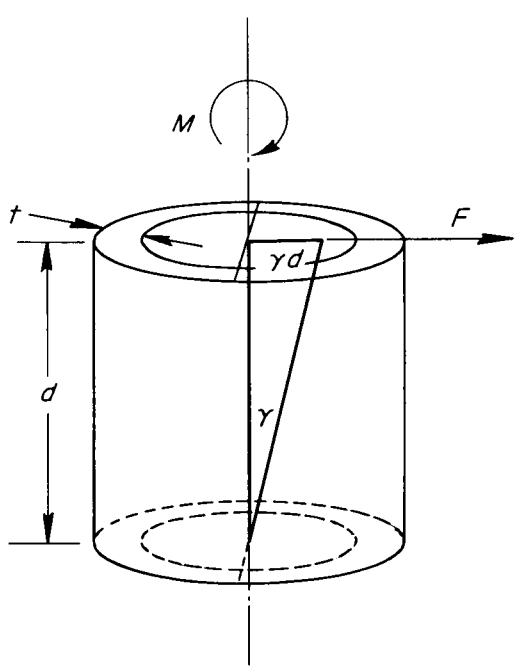

Fig. A.1. Force-Moment Diagram for Determining the Skirt Constants.

Thus

$$k_1 = \frac{F}{\gamma d} = \frac{GA}{d} \quad ,$$

where d is the height of the support skirt. If θ is the angle of rotation in radians,

$$\theta = \frac{Md}{EI_s} \quad .$$

Thus

$$C = \frac{M}{\theta} = \frac{EI_s}{d} \quad ,$$

where

$$I_s = \pi r^3 t \quad .$$

Verification that Eq. (23) Adequately Approximates Eq. (22)

In Eq. 22,

$$\frac{Mgh}{C} = 1.9 \times 10^{-4} \quad .$$

Thus,

$$C - Mgh \approx C \quad .$$

Substituting the appropriate constants into Eq. (22) gives

$$\ddot{\theta} + 26134\theta - 6546x - 0.04A = -6546S \quad .$$

Thus, the term containing A was also neglected.

APPENDIX B

Analog Solution of the Equations of Motion

For comparative and checking purposes, Eqs. (70), (71), and (72) were solved on an analog computer for values of δ_x, δ_A, and δ_θ of 0.05, 0.15, and 0.05, respectively.[1] The results of this analysis are given in Table B.1. Data from Table 2 are also given for comparison. The data given by Milligan are for a forcing function with a displacement amplitude of 0.075 ft; this implies that Milligan's results differ from the results of this report by a factor which is the ratio of 0.075 to 0.000467. As noted in Table B.1, the frequencies also varied slightly; however, the two sets of results are in good agreement. The ratios related to the x displacement in Table B.1 were not tabulated by Milligan, but they were derived from the curves presented. The ratios of the maximum displacement and acceleration associated with the x coordinate to the maximum ground displacement and acceleration are 1.64 from the analog solution and 1.65 from the exact solution.

The analog displacement results for a frequency of 58.43 radians per second are plotted for extended time intervals in Figs. B.1, B.2, and

[1]M. W. Milligan, An Analog Solution of the Seismic Vibrations of a Gas Cooled Reactor, ME-61-TN1, Engineering Experiment Station, University of Tennessee (July 1961).

Table B.1. Comparison of the Ratios of the Maximum Steady-State Displacements and Accelerations for Two Frequencies

Frequency (radians/sec)	$\frac{\max x}{\max S}$ or $\frac{\max \ddot{x}}{\max \ddot{S}}$		$\frac{\max A}{\max S}$ or $\frac{\max \ddot{A}}{\max \ddot{S}}$		$\frac{\max \theta(\text{radian})}{\max S}$ or $\frac{\max \theta(\text{radian})}{\max \ddot{S}}$	
	Analog Solution	Exact Solution	Analog Solution	Exact Solution	Analog Solution	Exact Solution
58.71[a]	1.10	1.19	9.05	8.4	0.120	0.097
100.7[b]	0.90	0.93	6.07	5.05	0.103	0.095

[a]The analog results are for 58.43 radians per second.

[b]The analog results are for 100.5 radians per second.

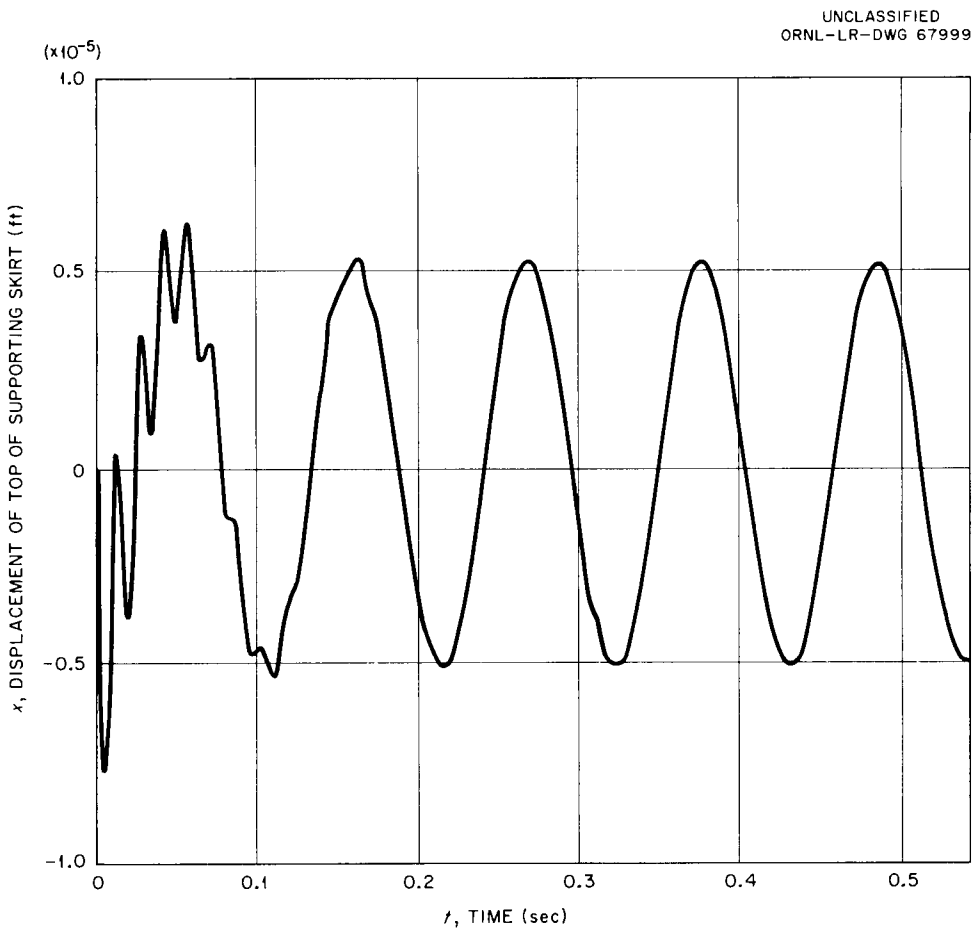

Fig. B.1. Time-Dependent Displacement of Top of Supporting Skirt (Analog Solution).

B.3. These figures contain the same information as Figs. 11, 12, and 13, respectively, as given by Milligan;[1] however, in Figs. B.1, B.2, and B.3 the vertical scale has been changed by a factor of 0.0062; i.e., the ratio of 0.000467 to 0.075.

In addition, Figs. B.1, B.2, and B.3 are comparable to Figs. 6, 7, and 8 of this report. The frequencies associated with each coordinate and the amplitudes of the transient displacements depicted in these figures are in good agreement, thus further indicating the agreement between the two methods of solutions.

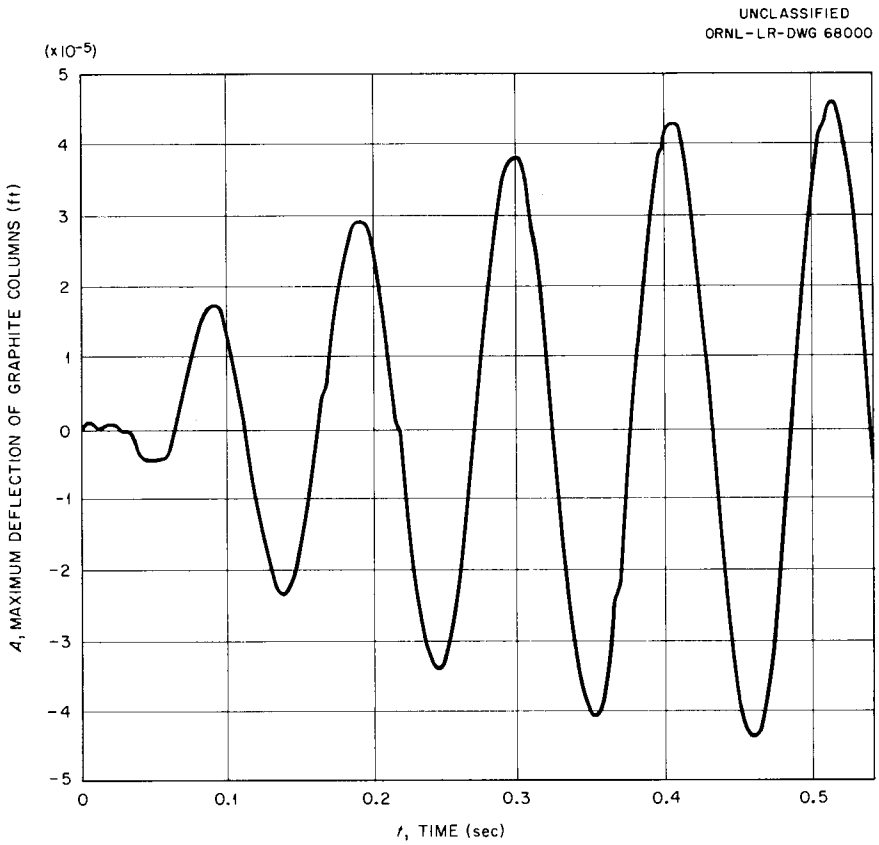

Fig. B.2. Time-Dependent Maximum Deflection in Graphite Columns (Analog Solution).

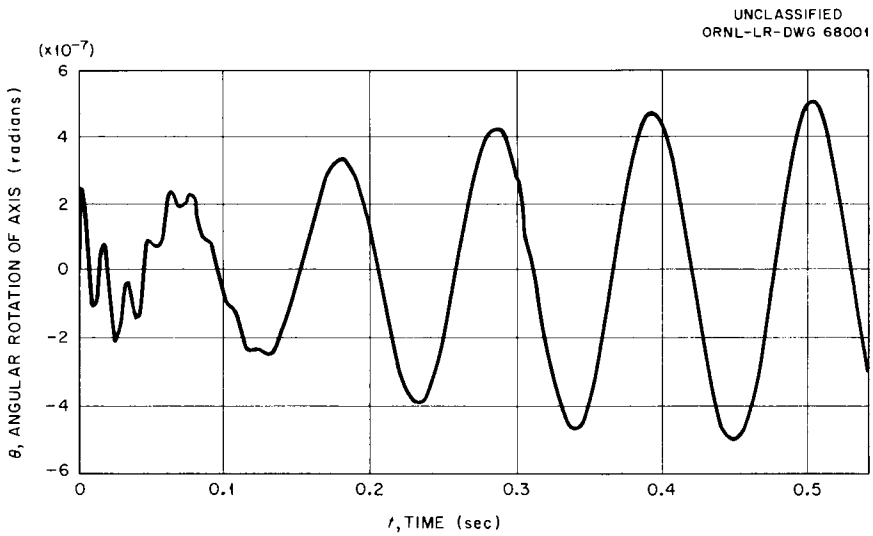

Fig. B.3. Time-Dependent Angular Rotation of the Axis of the Pressure Vessel (Analog Solution).

ORNL-3224

UC-80 — Reactor Technology
TID-4500 (17th ed.)

Internal Distribution

1. J. C. Amos
2. S. E. Atta
3. S. E. Beall
4. M. Bender
5. D. S. Billington
6. E. P. Blizard
7. A. L. Boch
8. C. J. Borkowski
9. E. J. Breeding
10. R. B. Briggs
11. H. P. Carter
12. R. H. Chapman
13. T. G. Chapman
14. R. D. Cheverton
15. C. W. Collins
16. J. M. Corum
17. J. A. Cox
18. D. A. Douglas
19. A. C. Downing
20. R. B. Evans
21. J. Foster
22. J. L. Fowler
23. A. P. Fraas
24. J. H. Frye, Jr.
25. C. H. Gabbard
26. W. R. Gall
27. E. A. Gift
28. D. R. Gilfillan
29. A. A. Grau
30-34. B. L. Greenstreet
35. W. R. Grimes
36. W. O. Harms
37. A. Hollaender
38. A. S. Householder
39. W. H. Jordan
40. P. R. Kasten
41. C. P. Keim
42. M. T. Kelley
43. B. W. Kinyon
44. J. A. Lane
45. C. E. Larson (K-25)
46. M. E. LaVerne
47. R. S. Livingston
48. M. I. Lundin
49. R. N. Lyon
50. H. G. MacPherson
51-70. W. D. Manly
71-73. R. L. Maxwell
74. J. T. Meador
75. A. J. Miller
76. S. E. Moore
77. K. Z. Morgan
78. I. K. Namba
79. M. L. Nelson
80. F. L. Parker
81. P. Patriarca
82. A. M. Perry
83. D. Phillips
84. C. A. Preskitt
85. M. E. Ramsey
86. G. C. Robinson
87. M. W. Rosenthal
88. G. Samuels
89. H. W. Savage
90. A. W. Savolainen
91. L. R. Shobe
92. O. Sisman
93. E. D. Shipley
94. M. J. Skinner
95. J. E. Smith
96. A. H. Snell
97. J. W. Snider
98. I. Spiewak
99. F. J. Stanek
100. J. A. Swartout
101. J. R. Tallackson
102. E. H. Taylor
103. D. B. Trauger
104. C. S. Walker
105. G. M. Watson
106. A. M. Weinberg
107. J. R. Weir
108. G. D. Whitman
109. B. W. Wieland

110-134. F. J. Witt
135-136. Central Research Library
137-139. Y-12 Technical Library Document Reference Section
140-163. Laboratory Records Department
164. Laboratory Records, RC

External Distribtuion

165-167. W. F. Banks, Allis-Chalmers Mfg. Co., Washington, D. C.
168. E. O. Bergman, National Engineering Science Co., Pasadena, California
169-171. P. D. Bush, Kaiser Engineers, Oakland, California
172-174. D. R. Carver, Louisiana State University, Baton Rouge, Louisiana
175. A. L. Chalfant, General Atomic, San Diego, California
176. R. A. Charpie, UCC Research Administration, New York, N. Y.
177-178. D. F. Cope, Reactor Division, AEC, ORO
179. B. Y. Cotton, Union Carbide Chemicals Co., Port Lavaca, Texas
180-181. R. W. Coyle, Vallecitos Atomic Laboratory
182. E. Creutz, General Atomic
183. W. E. Crowe, Los Alamos Scientific Laboratory, Los Alamos, New Mexico
184. F. T. Dodge, Carnegie Tech
185-187. R. B. Duffield, General Atomic
188. D. H. Fax, Westinghouse Atomic Power Division
189. G. W. Housner, California Institute of Technology, Pasadena, California
190. L. H. Jackson, AEC, ORO
191. M. Janes, National Carbon Research Laboratories, Cleveland, Ohio
192. T. Jarvis, Ford Instrument Co.
193. James R. Johnson, Minnesota Mining and Manufacturing Company, Saint Paul, Minn.
194. Richard Kirkpatrick, AEC, Washington
195. C. W. Kuhlman, United Nuclear Corp.
196. B. F. Langer, Bettis Plant, Westinghouse, Pittsburgh, Pennsylvania
197-198. H. Lichtenburger, General Nuclear Engineering Corp.
199. J. P. McGee, Bureau of Mines, Appalachian Experiment Station
200. R. W. McNamee, Manager, UCC Research Administration, New York, New York
201. R. Michel, Allis-Chalmers Mfg. Co., Washington, D. C.
202. R. L. Miller, Kaiser Engineers, Oakland, California
203. M. W. Milligan, University of Tennessee, Knoxville, Tennessee
204. S. G. Nordlinger, AEC, Washington
205. R. E. Pahler, High-Temperature Reactor Branch, Reactor Division, AEC, Washington
206. H. B. Rahner, Savannah River Operations Office
207. Corwin Rickard, General Atomic
208. W. A. Shaw, Auburn University, Auburn, Alabama
209. M. T. Simnad, General Atomic
210. H. L. Snider, Lockheed Aircraft Corporation, Marietta, Georgia
211. B. C. Sparks, University of Tennessee, Knoxville, Tennessee

212. Nathanial Stetson, Savannah River Operations Office
213. Donald Stewart, AEC, Washington
214. W. F. Swinson, Auburn University, Auburn, Alabama
215. Philip L. Walker, Pennsylvania State University
216. R. E. Watt, Los Alamos Scientific Laboratory
217-218. W. L. Webb, East Central Nuclear Group, Inc.
219. Division of Research and Development, AEC, ORO
220-820. Given distribution as shown in TID-4500 (17th ed.) under Reactor Technology Category (75 copies – OTS)